Hindawi Publishing Corporation
Mathematical Problems in Engineering
Volume 2015, Article ID 989260, 13 pages
http://dx.doi.org/10.1155/2015/989260

Research Article

A Numerical Study of Natural Convection Heat Transfer in Fin Ribbed Radiator

Hua-Shu Dou,[1] Gang Jiang,[2] and Lite Zhang[1]

[1]*The Province Key Laboratory of Fluid Transmission Technology, Faculty of Mechanical Engineering and Automation, Zhejiang Sci-Tech University, Hangzhou 310018, China*
[2]*Huadian Electric Power Research Institute, Hangzhou 310030, China*

Correspondence should be addressed to Hua-Shu Dou; huashudou@yahoo.com

Received 6 March 2014; Accepted 11 April 2014

Academic Editor: Zhijun Zhang

This paper numerically investigates the thermal flow and heat transfer by natural convection in a cavity fixed with a fin array. The computational domain consists of both solid (copper) and fluid (air) areas. The finite volume method and the SIMPLE scheme are used to simulate the steady flow in the domain. Based on the numerical results, the energy gradient function K of the energy gradient theory is calculated. It is observed from contours of the temperature and energy gradient function that the position where thermal instability takes place correlates well with the region of large K values, which demonstrates that the energy gradient method reveals the physical mechanism of the flow instability. Furthermore, the effects of the fin height, the fin number, and the fin shape on the heat transfer rate are also investigated. It is found that the thermal performance of the fin array is determined by the combined effect of the fin space and fin height. It is also observed that the effect of fin shape on heat transfer is insignificant.

1. Introduction

Natural convection heat transfer from finned surfaces has received much attention in both numerical simulations and experimental modeling, it is adopted extensively in various industrial devices, such as gas cooled nuclear reactors, automobile, aerospace vehicles, and electronic systems. Nowadays, as electronic equipment tends to be large as well as miniature, removing heat rapidly from the equipment is much more desirable than before, since the thermal efficiency of heat removal from the equipment can impact the life-span of the equipment. There are mainly two ways to enhance heat transfer from heat-generating electronic equipment. The first convenient method is to cool the electronic equipment by blowing air at a moderate velocity, and the second way is to use fin arrays. Since the forced convection approach has inherited problems and has to bear extra running cost, more and more researchers focus on designing optimum fin arrays, which can provide moderate heat transfer rates if designed properly.

In early stage, Starner and McManus [1] made some experiments by inserting four different rectangular fin arrays into a vertical, 45-degree plate and a horizontal plate, respectively. They obtained some free natural convection data which were widely used in the subsequent investigations. Harahap and McManus [2] obtained more detailed data by investigating free convection heat transfer from horizontal fin arrays using the schlieren shadowgraph technique. Jones and Smith [3] applied a Mach-Zender interferometer in their experiments to study the variation of local heat transfer coefficient for isothermal vertical fin arrays on a horizontal base. With a fixed fin height $L = 254$ mm, the experimental data shows that the overall heat transfer coefficient depends strongly on the fin space but weakly on the fin height. Rammohan Rao and Venkateshan [4] experimentally investigated the interaction of free convection and radiation in a horizontal fin array. The most important conclusion made in their research was that there was a mutual interaction between free convection and radiation and hence a simplistic approach based on additivity of radiation and convection heat transfer, calculated independently based on isothermal surfaces, was unsatisfactory. Yüncü and Anbar [5] also made some experiments to research the effects of the fin space, the fin height, and the temperature difference on heat transfer

with a fixed fin height and fin thickness. They found that there was an optimum fin spacing which was not related to the temperature difference. However, optimum fin spacing was inversely proportional with the fin height. Mobedi and Yüncü [6] numerically investigated the steady state natural convection heat transfer in longitudinally short rectangular fin arrays on a horizontal base. They observed two types of flow patterns. For the fin arrays with narrow fin spacing, air could only enter into the channel from the end regions. However, for the fin arrays with wide fin spacing, the air was also entrained into the channel from the region between the fins, turned 180 degrees at the base, and then moved up along the fin surface, while it flowed into the central part of the channel.

More recently, lots of researchers tried to enhance heat transfer rate of fin arrays using fin arrays. Arquis and Rady [7] investigated natural convection heat transfer and fluid flow characteristics from a horizontal fluid layer with finned bottom surface, and observed that the number of convection cells between two adjacent fins is a function of the values of the fin height and Rayleigh number. Liu [8] considered an optimum design problem for the longitudinal fin arrays with a constant heat transfer coefficient in a fuzzy environment, where the grid requirements to strictly satisfy the total fin volume and array width and maximize the heat dissipation rate are softened. Harahap et al. [9] conducted some experiments to investigate the effects of miniaturizing the base plate dimensions of vertically based straight rectangular fin arrays on the steady state heat dissipation performance under dominant natural convection conditions. They found that the relevant correlations proposed for large fin arrays were not applicable to the experimental data obtained from the miniaturized vertical rectangular fin arrays. Subsequently, Harahap et al. [10] conducted concurrent calorimetric and interferometric measurements to investigate the effect that the reduction of the base plate dimensions has on the steady state performance of the rate of natural convection heat transfer from miniaturized horizontal single plate-fin systems and plate-fin arrays. Their conclusions suggested that the fin height L and the fin number are the prime geometric variables for generalization. Dogan and Sivrioglu [11] experimentally investigated mixed convection heat transfer, and the results obtained showed that the optimum fin spacing which yielded the maximum heat transfer is S = 8-9 mm and the optimum fin spacing depends on the value of Ra. Azarkish et al. [12] used a modified genetic algorithm to maximize the objective function which is defined as the net heat transfer rate from the fin surface for a given height. Their results show that the number of the fins is not affected by the fin profile, but the heat transfer enhancement for the arrays with optimum fin profile is about 1–3 percent more than that for the arrays with conventional fin profiles. Giri and Das [13] numerically performed laminar mixed convection over shrouded vertical rectangular fin arrays attached to a vertical base. They found that the drop in pressure defect for forced convection, induced velocity for mixed convection and overall Nusselt number for mixed convection are correlated well with governing parameters of the considered problem. Wong and Huang [14] made some three-dimensional (3D) numerical simulations to investigate the effect of fin parameters on dynamic natural convection from long horizontal fin arrays. They observed that the optimum fin spacing decreases significantly with the fin height and increases slightly with the fin length. Furthermore, their observations agreed well with the results reported in the literature.

All the above experimental and numerical research focused on optimum design of the fin arrays in order to improve heat transfer rate. Almost all the related factors result in laminar convection involving low values of heat transfer coefficients. However, it is well known that the heat transfer rate will be prompted when the base flow loses its stability and flows in a turbulent manner [15]. Although some optimum fin arrays design can obtain a satisfying heat transfer rate which resulted from flow instability, the physical mechanism of flow instability of natural convection is still not fully understood. Recently, Dou et al. [16–24] suggested an energy gradient method which can reasonably reveal the physical mechanism of flow instability. Dou and Phan-Thien [16] described the rules of fluid material stability from the viewpoint of energy field. They claimed that the instability of natural convection could not be resolved by Newton's three laws, for the reason that a material system moving in some cases is not simply due to the role of forces. This approach explains the mechanism of flow instability from physics and derives the criteria of turbulence transition. Accordingly, this method does not attribute Rayleigh-Benard problem to forces, but to energy gradient. It postulates that when the fluid is placed on a horizontal plate and is heated from below, the fluid density in the bottom becomes low which leads to an energy gradient $\partial E/\partial y > 0$ along y-coordinate. Only when $\partial E/\partial y$ is larger than a critical value will the flow become unstable and then fluid cells of vorticities will be formed. More recently, Dou et al. [25] applied the energy gradient method to natural convection and the results from numerical simulations accord well with those predicted based on the criteria originated from energy gradient method.

This study is focused on the research of effects of fin arrays parameters on convection heat transfer coefficient. Then, the energy gradient method is employed to reveal the physical mechanism of flow instability and explain the reason why the optimum fin arrays can result in better heat transfer rate.

2. Computational Geometry and Numerical Procedures

2.1. Computational Geometry. The computational geometry is shown in Figure 1. Here, the geometry is simplified from the 3D solid of GH-4 ribbed radiator model [26]. The simplified cavity in this study is a two-dimensional (2D) square, in which the length of the square cavity is 250 mm, and the origin of the coordinates is at the lower left corner of the cavity. The fin arrays are fixed at the hot bottom of the cavity with an equal distance. Here, S is the fin space, H is the fin height, and H and S are variable. In addition, f_t means the thickness of the fin arrays which is fixed at 2 mm in this study and can be neglected by comparing to the fin height and the length of the cavity, while b_t means the thickness of the bottom plate which is equal to 3 mm.

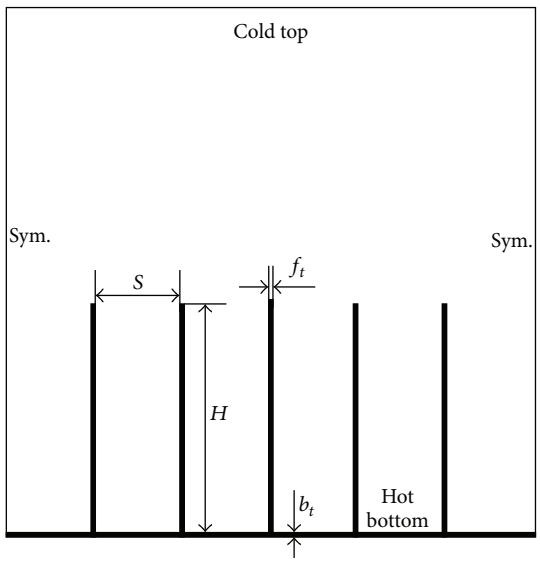

Figure 1: Numerical geometry.

The computational geometry is divided into two areas, which contains a solid area and a fluid area. The solid area includes the fin arrays and the base plate, in which the material is copper, while the rest of the geometry is the fluid area where the air fills in it. All the walls of the cavity are solid and no-slip. The wall style of the left and the right walls of the cavity is symmetric. The top wall of the cavity is given a fixed temperature of 300 K, and the base of the plate is given a fixed temperature of 360 K. Furthermore, the fluid area is given an initial temperature of 300 K.

2.2. Governing Equations. For the problem described in the previous section, the development of natural convection in the fluid area is governed by the following continuity equations, two-dimensional steady Navier-Stokes equations and an energy equation. The heat transfer in the solid area is governed by a heat conduction equation. All these equations are based on Boussinesq approximation and listed as follows:

$$\frac{\partial u}{\partial x} + \frac{\partial v}{\partial y} = 0,$$

$$\frac{\partial u}{\partial t} + u\frac{\partial u}{\partial x} + v\frac{\partial u}{\partial y} = -\frac{1}{\rho}\frac{\partial p}{\partial x} + \upsilon\left(\frac{\partial^2 u}{\partial x^2} + \frac{\partial^2 u}{\partial y^2}\right),$$

$$\frac{\partial v}{\partial t} + u\frac{\partial v}{\partial x} + v\frac{\partial v}{\partial y} = -\frac{1}{\rho}\frac{\partial p}{\partial y} + \upsilon\left(\frac{\partial^2 v}{\partial x^2} + \frac{\partial^2 v}{\partial y^2}\right) + g\beta\left(T - T_0\right),$$

$$\frac{\partial T}{\partial t} + u\frac{\partial T}{\partial x} + v\frac{\partial T}{\partial y} = k\left(\frac{\partial^2 T}{\partial x^2} + \frac{\partial^2 T}{\partial y^2}\right),$$

$$\frac{\partial^2 T}{\partial x^2} + \frac{\partial^2 T}{\partial y^2} = 0, \tag{1}$$

where x and y are the horizontal and vertical coordinates, t is the time, T is the temperature, p is the pressure, u and v are the velocity components in the x and y directions, respectively, g is the acceleration due to gravity, β is the coefficient of thermal expansion, ρ is the fluid density, k is the thermal diffusivity, and υ is the kinematic viscosity.

2.3. Numerical Algorithm. The governing equations (1) are implicitly solved using a finite-volume SIMPLE scheme, with the QUICK scheme approximating the advection term. The diffusion terms are discretized using central differencing with a second-order accuracy. The discretized equations are iterated with the specified underrelaxation factors. In addition, it should be noted that the flow is steady.

In this study, the mean value of the local Nusselt number along the top cold wall is calculated for measuring heat transfer performance as follows:

$$\mathrm{Nu} = \frac{1}{L}\int_0^L \left(\frac{\left|\partial T/\partial y\right|_{y-L}}{\Delta T/L}\right) dx = \frac{1}{\Delta T}\int_0^L \left|\frac{\partial T}{\partial y}\right|_{y-L} dx \tag{2}$$

Here, λ is the thermal conductivity, ΔT is the temperature difference, and c_p is the specific heat capacity.

3. Grid Independent Test

In order to examine the independence of the gird size to the computing result, three different sized meshes are constructed. Here, grid (a) is uniformly meshed with $\Delta x = 0.004$ mm, grid (b) is uniformly meshed with $\Delta x = 0.002$ mm, and grid (c) is uniformly meshed with $\Delta x = 0.001$ mm.

Figure 2 shows the temperature contours in three different mesh sizes. It can be quantitatively observed that the temperature contours are almost the same in three different mesh sizes by making a comparison. Figure 3 shows the temperature versus iterations at the same monitor point with the three different mesh sizes. It can be found that the temperature difference is getting smaller as the difference of the mesh size is getting smaller. Furthermore, for the two finer meshes the difference of the steady-state temperature is negligible. In what follows, the medium (or fine) mesh resolution is adopted for all the calculations.

4. Application of Energy Gradient Method

4.1. Energy Gradient Method. It is observed in Figure 2 that the base flow loses its stability by forming vorticities and by moving with a wave form, which is helpful to enhance heat transfer. However, the physical mechanism of the flow instability of natural convection is still not fully understood. Energy gradient method will be applied in natural convection to explain the physical mechanism of flow instability in this study.

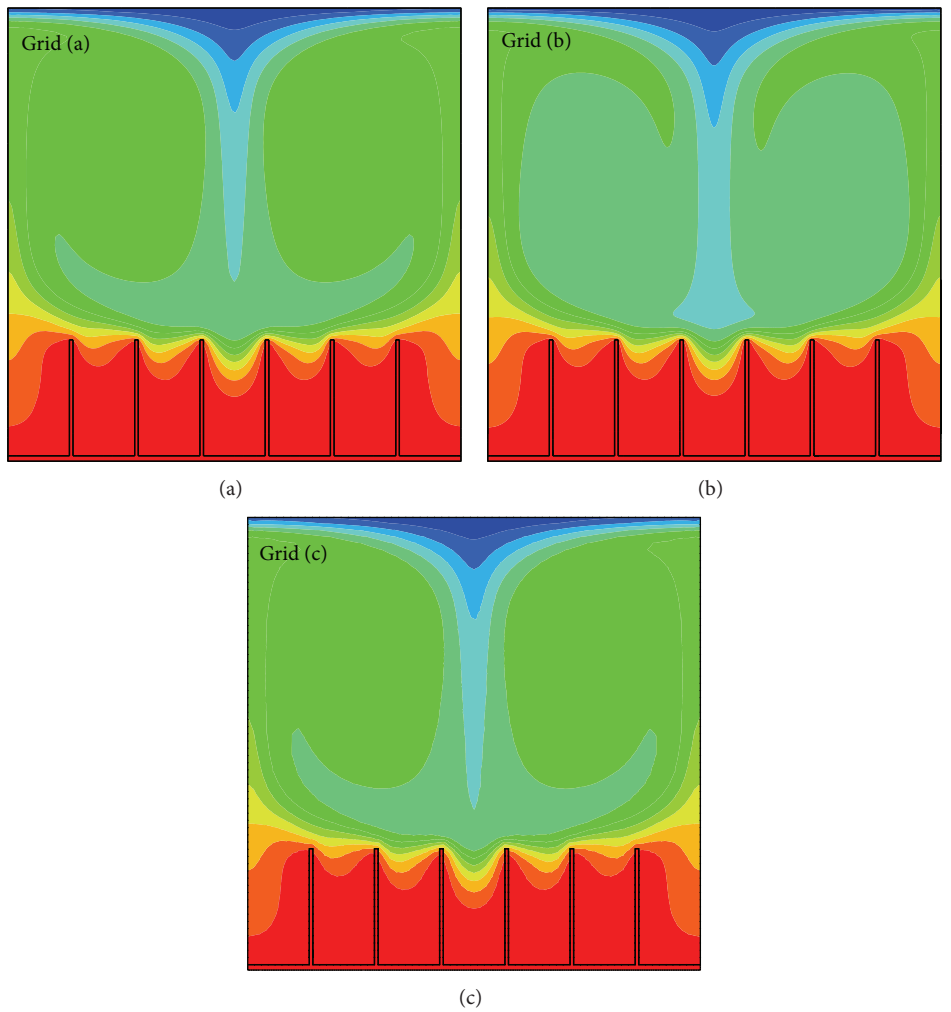

Figure 2: Temperature contours with three different meshes: grid (a) $\Delta x = 0.004$ mm, grid (b) $\Delta x = 0.002$ mm, and grid (c) $\Delta x = 0.001$ mm.

Dou et al. [16–24] suggested an energy gradient method which can be treated as the criteria of flow instability. And the criteria of flow instability can be expressed as follows:

$$F = \frac{\Delta E}{\Delta H} = \frac{(\partial E/\partial n)\left(2\overline{A}/\pi\right)}{(\partial H_s/\partial s)(\pi/\omega_d)u} = \frac{2}{\pi^2}K\frac{\overline{A}\omega_d}{u} = \frac{2}{\pi^2}K\frac{v'_m}{u} < \text{Const}, \tag{3}$$

where

$$K = \frac{\partial E/\partial n}{\partial H_s/\partial s}. \tag{4}$$

Here, u is the streamwise velocity of main flow, $\overline{A}$ is the amplitude of the disturbance distance, ω_d is the frequency of the disturbance, $v'_m = \overline{A}\omega_d$ is the amplitude of the disturbance of velocity, and π is the circumference ratio. Furthermore, F is a function of coordinates which expresses the ratio of the energy gained in a half-period by the particle and the energy loss due to viscosity in the half-period. K is a dimensionless field variable (function) and means the ratio of the transversal energy gradient and the rate of the energy loss along the streamline. H_s is the loss of the total mechanical energy per unit volumetric fluid along the streamline for finite height. Here, $E = p + 1/2\,\rho V^2$ expresses the total mechanical energy per unit volumetric fluid, s is along the streamwise direction, and n is along the transverse direction.

4.2. Application of Energy Gradient Method in Natural Convection. In the present study, we will use the energy gradient function K to reveal the physical mechanism of flow instability in natural convection. The fluid fills in a 2D simplified fin radiator model and the base flow is initially stationary. Based on the energy gradient method and the particular condition of the base flow, the energy gradient function K of natural convection can be expressed as follows:

$$K = \sqrt{\left(\frac{\partial E}{\partial x}\right)^2 + \left(\frac{\partial E}{\partial y}\right)^2}. \tag{5}$$

It should be noted that the influence of the gravitational energy is neglected in terms of the total mechanical energy in

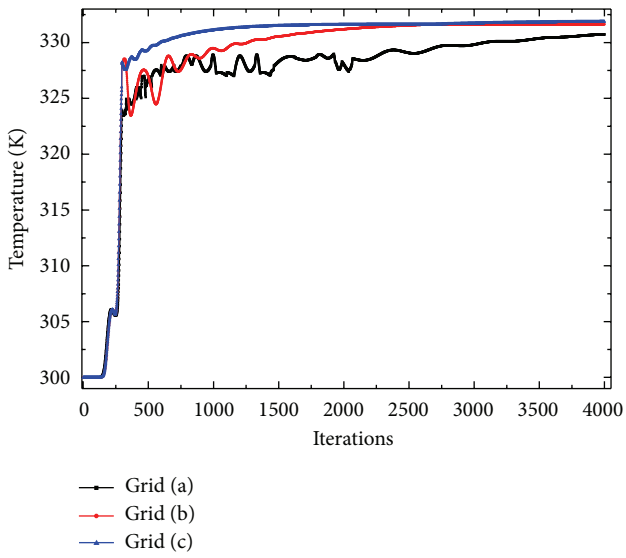

Figure 3: Temperature profile calculated with three different grid meshes: grid (a) $\Delta x = 0.004$ mm, grid (b) $\Delta x = 0.002$ mm, and grid (c) $\Delta x = 0.001$ mm.

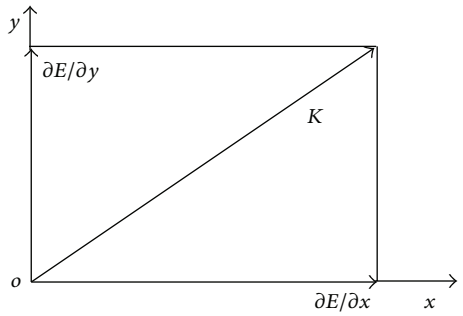

Figure 4: Calculation of K.

this study since the fluid is air; then $E \sim p_0$ is obtained; consequently the energy gradient function K of transient natural convection can be written as $K = \sqrt{(\partial p_0/\partial x)^2 + (\partial p_0/\partial y)^2}$, which is shown in Figure 4. Here, p_0 represents the total pressure.

5. Results and Discussions

5.1. Physical Mechanism of Flow Instability. Patterson and Imberger [15] announced that the flow instability could enhance heat transfer rate of natural convection, and the heat transfer rate increases with the addition of the intensity of flow instability. In the following, the physical mechanism of flow instability will be discussed using the energy gradient method.

Figures 5(a) and 5(b) show the contours of velocity and total pressure respectively with iterations of 4000. The following observations can be made in Figure 5(a). Firstly, the velocity in the whole flow field distributes symmetrically along the vertical center line. Secondly, the magnitude of velocity near the left and right walls and in the center of the cavity is relatively large, while the velocity between the adjacent fins is very weak. This large velocity difference in the cavity is due to the variation of the heat transfer modes. The reason why the velocity near the left and right walls and in the center of the cavity is large is that the heat flux is focused in these areas and moves downward driven by the buoyancy. However, the heat flux between the adjacent fins is rare and the buoyancy can be neglected attributed to the small temperature difference between adjacent fins; hence the velocity between adjacent fins is very weak. Thirdly, there are two blue areas where the velocity is very weak above the fin arrays. This is due to the convection of heat along the symmetrical wall, and these blue areas are not affected evidently by convection.

Similarly, the findings from Figure 5(b) can be summarized as follows. Firstly, the total pressure decreases gradually from the top to the bottom. The fluid flow and the heat flux along the symmetrical wall move upward driven by the buoyancy and concentrates near the top wall of the cavity; thus the total pressure difference will be produced. Secondly, two circulating regions occur symmetrically above the fin arrays. This is due to the circulation flow of the heat flux along the symmetrical walls. Thirdly, the total pressure gradient is irregular above the fin arrays, while the total pressure gradient between the adjacent fins is regular. The circulation flow of heat flux above the fin arrays which results in the irregular distribution of total pressure gradient. The regular gradient distribution between the fins is attributed to the symmetrical movement of heat flux along the fin arrays surfaces and the weak buoyancy between the fins.

Figures 6(a) and 6(b) show the contours of temperature and the contours of the value of K at the iterations of 4000, respectively. It can be seen in Figure 6(a) that the base flow downstream of the fin loses its stability forming small vorticities and by moving in a wave form. It can be seen in Figure 6(b) that the value of K in the red area and the yellow area is much higher than that in other areas. In the meantime, there exist two symmetrical green areas with high value of K on the trajectory of the heat flux circulation. Based on the criteria of flow instability of the energy gradient method, there is a critical value K_c, above which the flow will lose its stability. Thus, the flow instability could most likely occur in the red, yellow, and green areas. Making a further comparison between Figures 6(a) and 6(b), it is easy to observe that the positions where instabilities take place are in accordance with the area with the higher value of K. This phenomenon indicates that the application of the energy gradient method in the simplified mode of ribbed radiator is reliable, and the energy gradient method can reveal the physical mechanism of flow instability of natural convection.

Moreover, it can be found that the regions with high velocity magnitude accord well with the areas with large value of K. Consequently, the flow instability of natural convection has an instinct affection on the velocity of the fluid flow.

5.2. Effect of Fin Height. In order to investigate the effect of fin height on heat transfer rate, here two groups of fin arrays are chosen for comparison. In the first group, all the

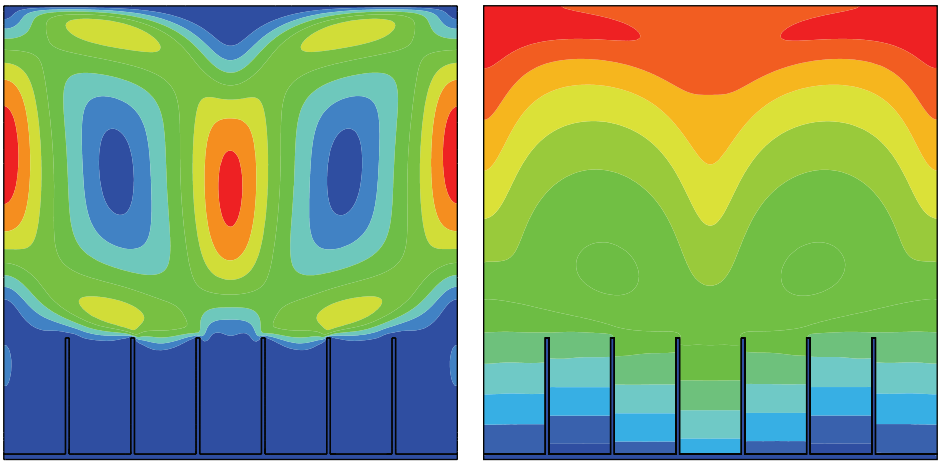

(a) Velocity contours (b) Total pressure contours

Figure 5: Velocity contours and total pressure contours, $H = 65$ mm.

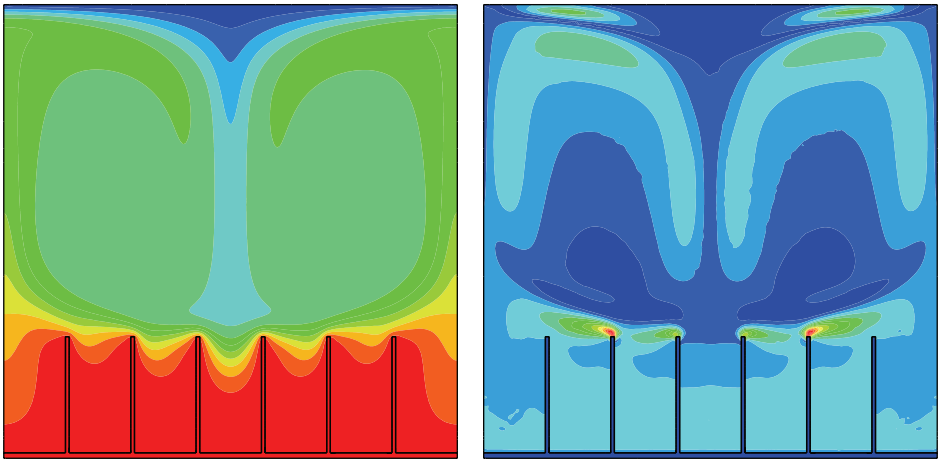

(a) Temperature contours (b) K contours

Figure 6: Validation of energy gradient method, $H = 65$ mm.

fin spaces are fixed at 61 mm, and the fin height changes from 25 mm to 105 mm with an equal increment of 20 mm. In the second group, all the fin spaces are fixed at 26 mm and the fin height changes over the same range in the first group. In the following section, the Nusselt number is selected to represent the heat transfer rate.

Figure 7 shows the temperature contours and contours of the value of K with different fin height where the fin space is fixed at 61 mm. Figure 8 shows the temperature contours and contours of the value of K with different fin height where the fin space is fixed at 26 mm. Table 1 shows the Nusselt number in different numerical cases. It is easy to observe the following results by comparing Figures 7 and 8 and Table 1. Firstly, Figures 7 and 8 show that the areas where flow instabilities occur in temperature contours accord well with the region where the value of K is very large in contours of the value of K. These results validate the criteria of flow instability based on the energy gradient method, which in turn demonstrates that the application of energy gradient method to natural convection is reasonable. Secondly, it is found that the intensity of flow instability changes dramatically in Figure 7 when the fin height changes from 45 mm to 65 mm with a fixed fin space of 61 mm. It also means that the heat transfer rate will be increased fiercely. However, it is found in Figure 8 that the flow instability varies in a very small range, which means that the variation of heat transfer rate is limited. At the same time, it is found from the second row of Table 1 that the variation range of Nusselt number is notable, while the Nusselt number alters within a limited extent detected from the third row of Table 1. This accordance between flow instability and heat transfer rate validates the hypothesis made by Patterson and Imberger [15]. The heat transfer rate increases with the addition of the intensity of flow instability. Thirdly, it is found in Figure 7 that the heat flux moves right by jumping over the fins when the fin height is 25 mm and 45 mm, respectively, whereas the flux

Table 1: Effect of fin height, H and S mean fin height and fin space respectively.

Nu	$H = 25$ mm	$H = 45$ mm	$H = 65$ mm	$H = 85$ mm	$H = 105$ mm
$S = 61$ mm	1.92	1.97	2.35	2.35	2.34
$S = 26$ mm	2.37	2.38	2.38	2.39	2.39

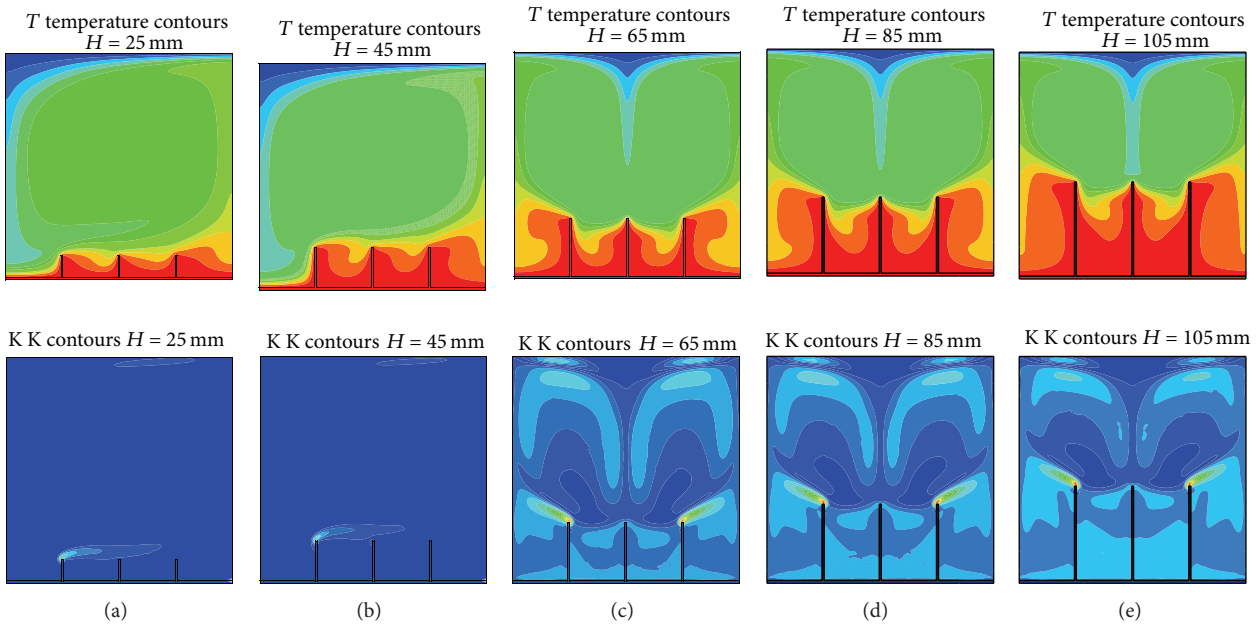

Figure 7: Temperature contours and contours of the value of K with different fin heights where fin space is fixed at 61 mm: (a) $H = 25$ mm, (b) $H = 45$ mm, (c) $H = 65$ mm, (d) $H = 85$ mm, and (e) $H = 105$ mm.

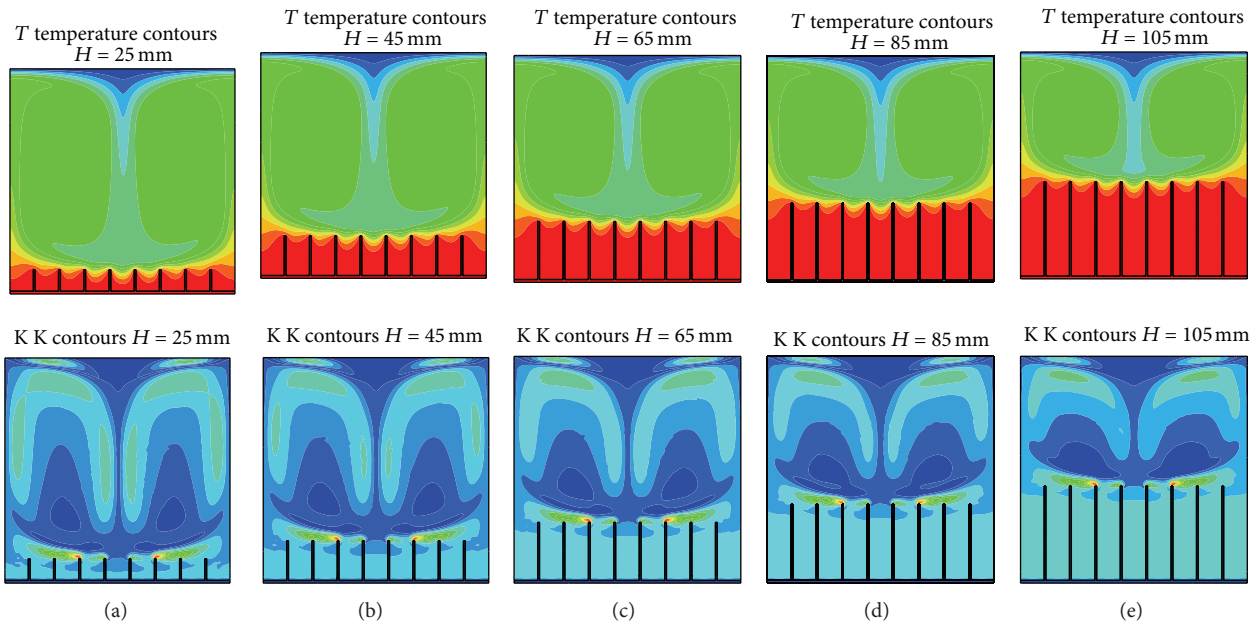

Figure 8: Temperature contours and contours of the value of K with different fin heights where fin space is fixed at 26 mm: (a) $H = 25$ mm, (b) $H = 45$ mm, (c) $H = 65$ mm, (d) $H = 85$ mm, and (e) $H = 105$ mm.

Table 2: Effect of fin space, H and S mean fin height and fin space, respectively.

Nu	$S = 82$	$S = 61$	$S = 48.4$	$S = 40$	$S = 34$	$S = 29.5$	$S = 26$	$S = 23.2$
$H = 45$ mm	2.76	1.97	2.37	2.27	2.30	2.32	2.38	2.42
$H = 85$ mm	2.95	2.36	2.38	2.28	2.31	2.35	2.39	2.43

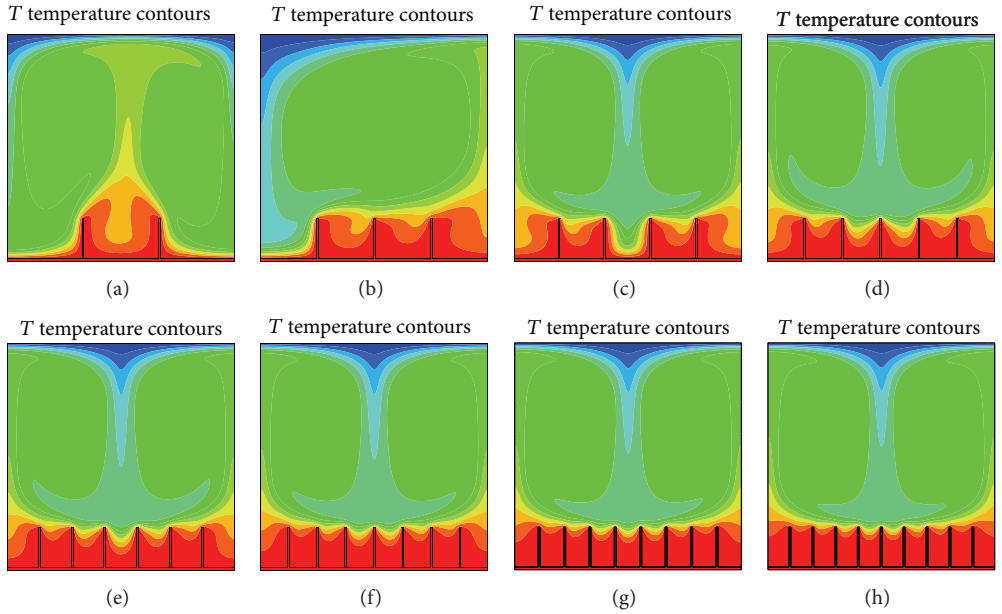

Figure 9: Temperature contours with a fixed fin height of 45 mm and the fin space changes from 82 mm to 23.2 mm characterized by the increase of fin number (n): (a) $n = 2$, (b) $n = 3$, (c) $n = 4$, (d) $n = 5$, (e) $n = 6$, (f) $n = 7$, (g) $n = 8$, and (h) $n = 9$.

moves upward along the symmetric wall when the fin height is 65 mm, 85 mm, and 105 mm, respectively. It is observed in Figure 8 that the heat flux moves upward symmetrically in all the numerical cases. The difference of flow behavior is jointly affected by the fin height and the fin space. When the fin height is small, the heat flux jumps over the fins driven by the buoyancy. When the fin height is small, the buoyancy between the fins is weak, and it is not very easy for the heat flux to jump over the fins. In addition, when the fin space reduces characterized by the increase of the fin number, the difficulty for the heat flux jumps over the fins will increase. Moreover, the temperature difference between adjacent fins is very weak which results in a negligible buoyancy between adjacent fins. Thus, the decrease of the fin space reduces the driven force, which is needed for the heat flux to jump over the fins.

It is summarized from the above discussion that the flow behavior is dominated by the combined influences of fin space and fin height, which affects the heat transfer rate ultimately. The influences on heat transfer rate can be explained with the energy gradient theory.

5.3. Effect of Fin Space. Two sets of numerical cases are selected to study the effect of fin space on flow instability or heat transfer rate. In the first set of numerical cases, the fin height is fixed at 45 mm, and the fin space decreases characterized by the increasing of the fin number. In the second set of numerical cases, the fin height is fixed at 85 mm and the fin space decreases characterized by the same pattern in the first set. Figures 9 and 10 show the temperature contours and contours of the value of K for the first set of numerical cases described above, in which all the fin heights are given as 45 mm. Figures 11 and 12 show the temperature contours and contours of the value of K for numerical cases, in which all the fin heights are fixed at 85 mm. Table 2 lists the Nusselt number of different numerical cases.

Comparing Figures 9–12 and Table 2, some observations can be obtained. Firstly, when the fin number is 2, the strongest intensity of flow instability occurs, which possesses the most efficient heat transfer rate. The heat flux focuses in the center of the cavity, and it moves upward along the vertical center line of the cavity. Once the largely extracted heat flux loses its stability and spreads randomly, the intensity of flow instability is much stronger than any other patterns of flow instability. Secondly, Figures 9 and 10 indicate that the intensity of flow instability is very weak when the fin number is 3. However, the intensity difference of flow instability can be neglected when the fin number is larger than 3. This result can be validated by the data in Table 2. When the fin number is 3, the heat flux moves right by jumping over the fins and focuses in the adjacent fins near the right wall. Hence, little heat flux moves upward, which results in a weak intensity of flow instability. However, the heat fluxes in all the cavities move upward symmetrically, which results in

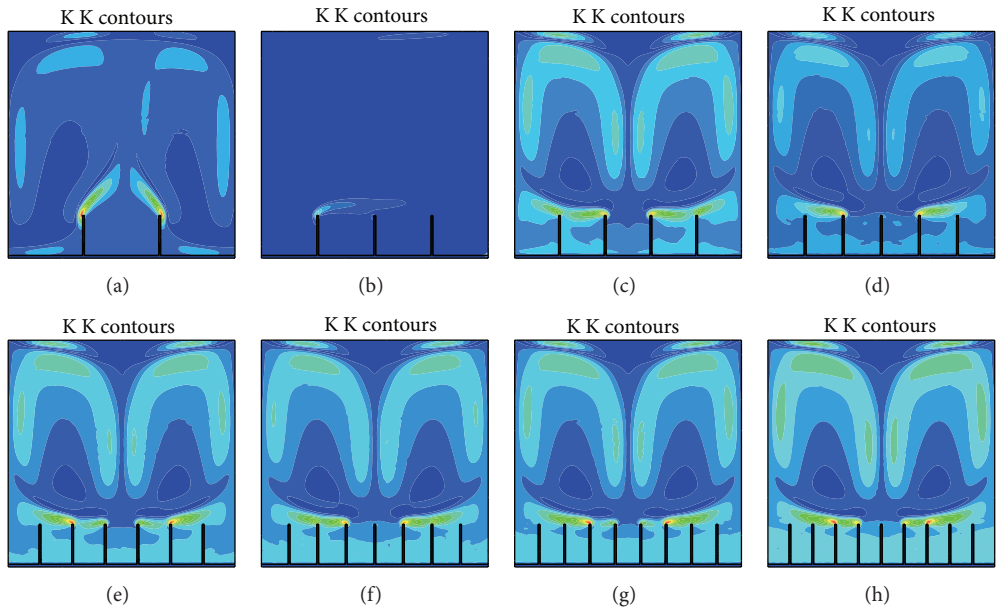

FIGURE 10: Contours of the value of K with a fixed fin height of 45 mm and the fin space changes from 82 mm to 23.2 mm characterized by the increase of fin number (n): (a) $n = 2$, (b) $n = 3$, (c) $n = 4$, (d) $n = 5$, (e) $n = 6$, (f) $n = 7$, (g) $n = 8$, and (h) $n = 9$.

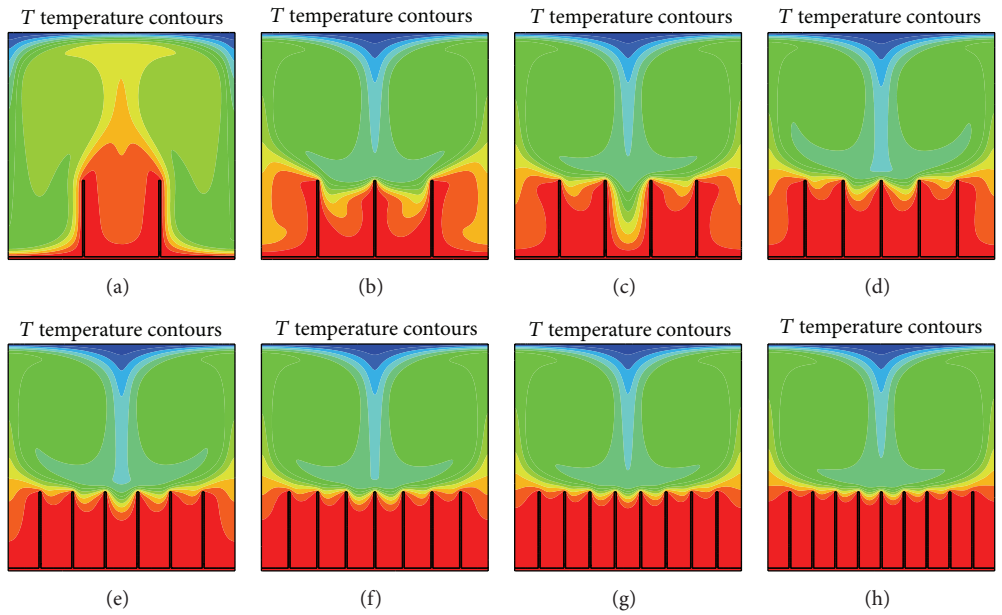

FIGURE 11: Temperature contours with a fixed fin height of 85 mm and the fin space changes from 82 mm to 23.2 mm characterized by the increase of fin number (n): (a) $n = 2$, (b) $n = 3$, (c) $n = 4$, (d) $n = 5$, (e) $n = 6$, (f) $n = 7$, (g) $n = 8$, and (h) $n = 9$.

a negligible heat transfer rate when the fin number is more than 3. Thirdly, it is easy to find that the intensity of flow instability changes slightly when the fin number is more than 2 by comparing Figures 11 and 12 and Table 2. This can be attributed to the effect of fin space. When the fin space is large, the convection between adjacent fins plays a leading role and it can trigger flow instability. Meanwhile, more heat flux focuses between adjacent fins and little heat flux moves upward; thus the flow instability will be restricted. When the fin space is small, the heat conduction between adjacent fins plays a leading role and it restricts flow instability. At the same time, more heat flux moves upward which results in stronger flow instability. The change of the fin space results in the change of specific weight of the heat conduction and heat convection between adjacent fins, as well as the change of the accumulation of heat flux between adjacent fins. At last, the intensity of flow instability changes slightly.

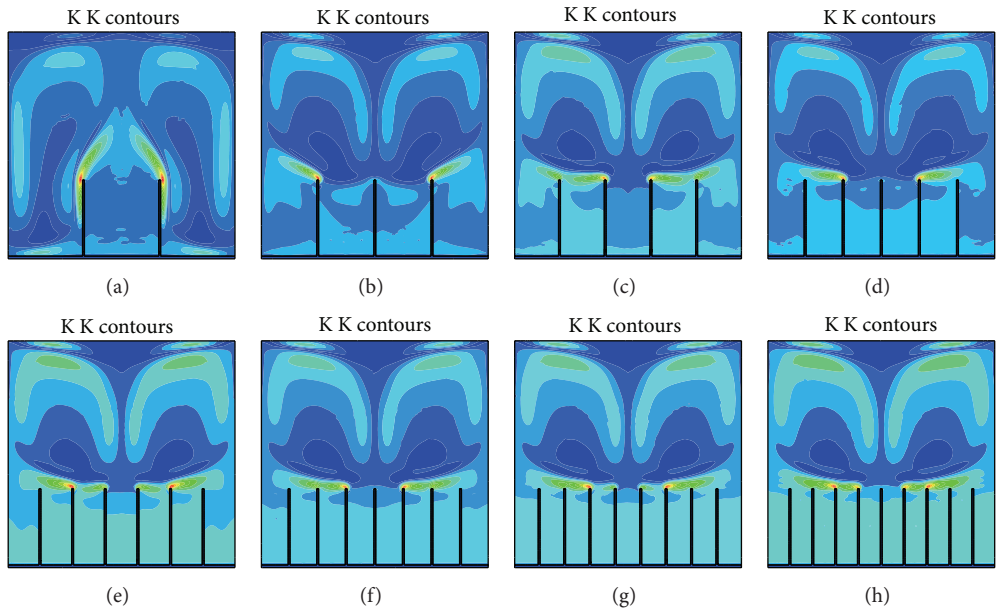

Figure 12: Contours of the value of K with a fixed fin height of 85 mm and the fin space changes from 82 mm to 23.2 mm characterized by the increase of fin number (n): (a) $n = 2$, (b) $n = 3$, (c) $n = 4$, (d) $n = 5$, (e) $n = 6$, (f) $n = 7$, (g) $n = 8$, and (h) $n = 9$.

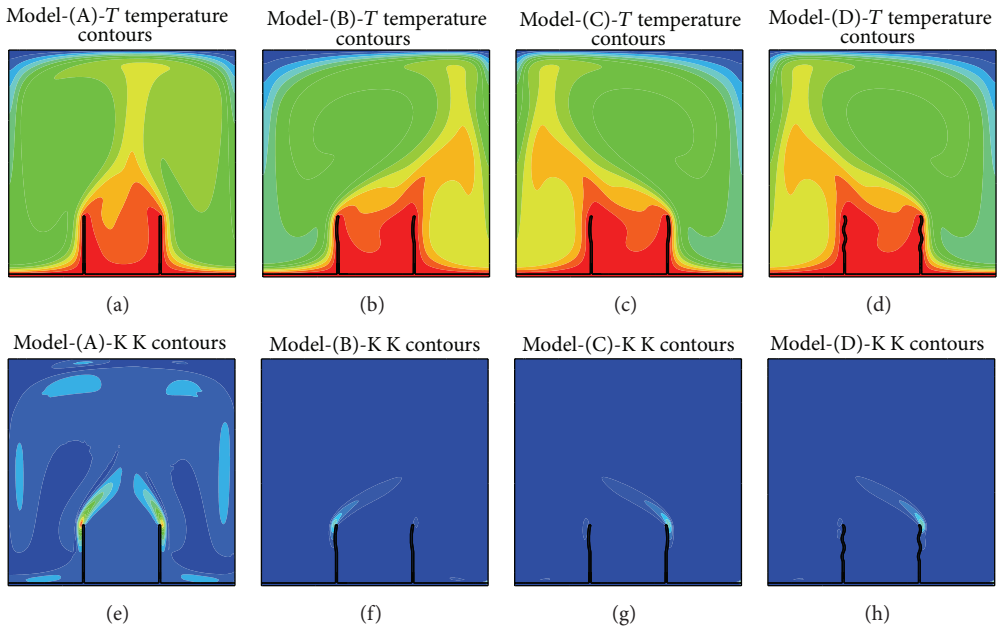

Figure 13: Temperature contours and contours of the value of K in different fin shape with a fixed fin space of 82 mm.

Consequently, in addition to the validation of criteria of flow instability based on the energy gradient method, another two conclusions can be summarized as follows. (1) The cavity possesses the most efficient heat transfer rate when the fin number is 2. (2) The change of the fin space results in the change of the specific weight of heat conduction and heat convection as well as the accumulation of heat flux between adjacent fins; hence the heat transfer rate changes slightly.

5.4. Effect of Fin Shape. In this part, the effect of the fin shape on flow instability or heat transfer rate is discussed. The straight fin arrays are chosen as the base group as model-(A) shown in Figure 13. The shapes of models-(B–D) shown in Figure 13 are all different from each other and a fixed fin space of 26 mm is chosen for all cases. The fin arrays in model-(B) are curved for one piece in the same direction with a radius of 70 mm. The fin arrays in model-(C) are curved for one piece with a radius of 70 mm, which are fixed symmetrically. The fin arrays in model-(D) are curved for four pieces with a radius of 10 mm.

Figures 13–15 show the temperature contours and contours of the value of K when the fin space is 82 mm, 48.4 mm,

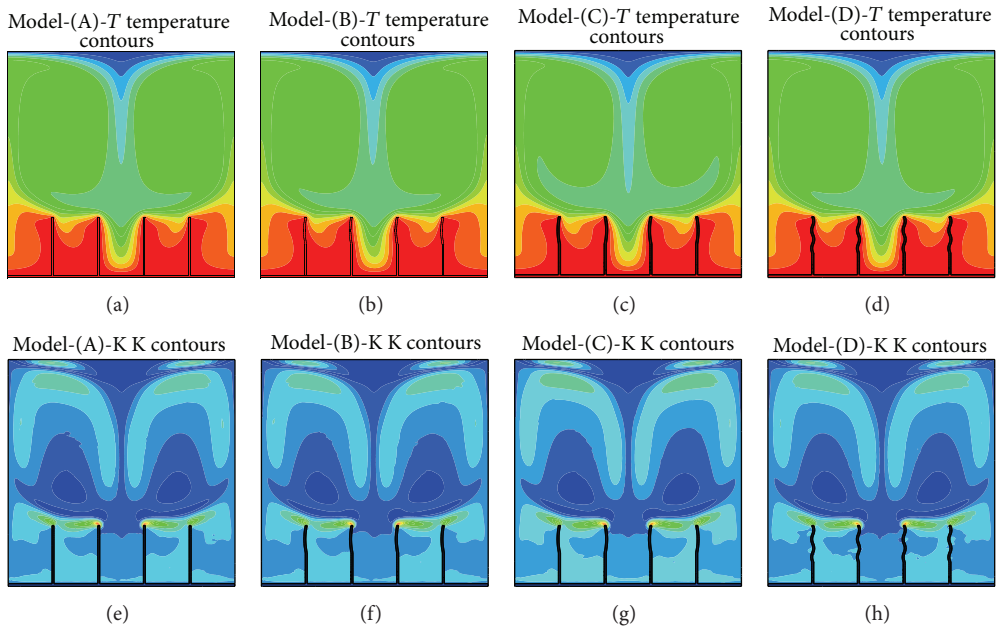

Figure 14: Temperature contours and contours of the value of K in different fin shape with a fixed fin space of 48.4 mm.

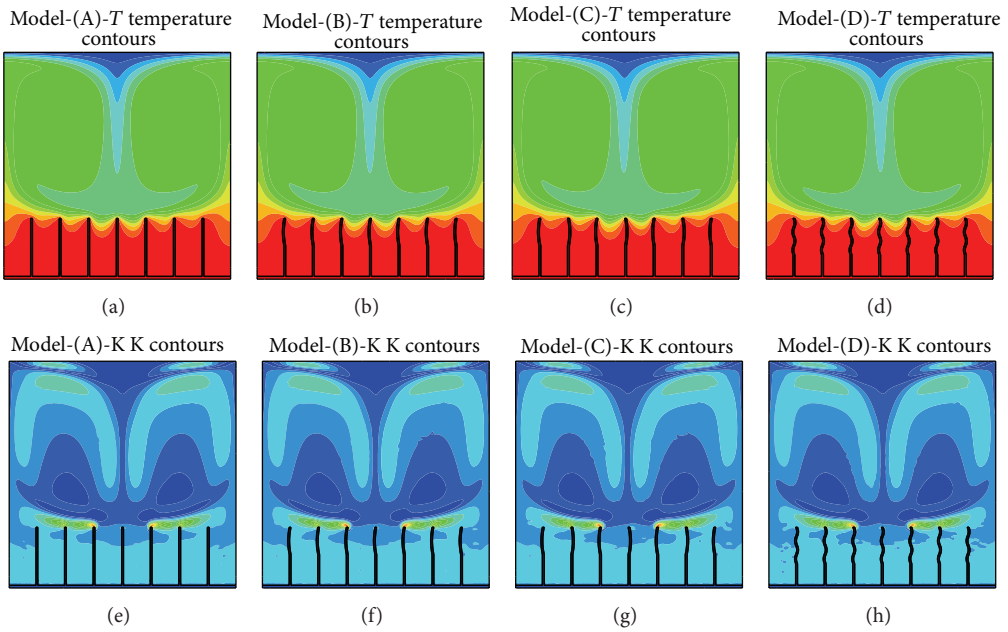

Figure 15: Temperature contours and contours of the value of K in different fin shape with a fixed fin space of 29.5 mm.

and 29.5 mm, respectively. Figure 16 shows the heat transfer rate obtained with four different fin shapes, and fin space is characterized by the fin number.

It is easy to get the following results by comparing Figures 13–15 to Figure 16. Firstly, it is found in Figure 13 that the largest intensity of flow instability occurs in model-(A), and the intensity difference in other models can be neglected. These results accord well with the data in Figure 16. This is attributed to the effect of fin shape, which results in the different form of flow instability. Convection occurs mainly in the center of the cavity and spreads around and produces a large intensity of flow instability. However, the heat fluxes in models-(B–D) move upward symmetrically and produce relatively small flow instability. Thus, this result is validated in Figure 16, which shows that the most efficient heat transfer rate occurs in model-(A) when the fin space is 82 mm. Secondly, it is found in Figure 14 that the flow instability in model-(C) is very weak, and the intensity variation of flow instability in other models is very small. This heat transfer rate difference is due to the bent direction of the fins.

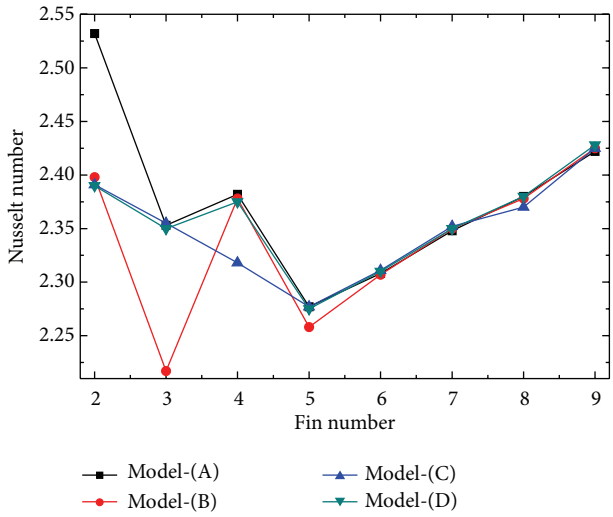

Figure 16: Nusselt number versus fin space characterized with fin number in different fin shape.

The symmetrically bent fins in model-(C) will restrict the movement of the heat flux above the fin arrays, thus reduce the intensity of flow instability. The fins in other models are either curved in the same direction or are straight, which has a limited effect on the variation of the heat transfer modes (i.e. convection versus conduction). Thus the intensity difference of flow instability is not distinct. Comparing these results to the data in Figure 16, it is easy to make a conclusion that the symmetrically bent fins can reduce the heat transfer rate when the fin space is fixed at 48.4 mm. Thirdly, it is observed in Figure 15 that the intensity of flow instability in four different fin shapes is almost the same, which is confirmed in Figure 16. The heat convection in adjacent fins is very weak when the fin space is 29.5 mm, and it is not easy for the weak heat convection to trigger flow instability.

Some observations can be summarized as follows by comparing Figures 13–15 to Figure 16. Firstly, the model with straight fins possesses the most efficient heat transfer rate. Secondly, the model with symmetrically bent fins can restrict heat transfer rate when the fin space is 48.4 mm. Thirdly, the heat transfer rate is dominated by the fin space, not by the fin shape, when the fin space is 29.5 mm.

6. Conclusions

In this paper, the convection and heat transfer rate behaviors of fin arrays are studied based on the criteria of flow instability derived from energy gradient method. All the numerical procedures are based on steady Navier-Stokes equations and Boussinesq approximation. The effect of fin height, fin space, and fin shape on heat transfer rate and flow instability are examined. The physical mechanism of flow instability and the relationship between flow instability and heat transfer rate are analyzed. Conclusions can be drawn as follows.

(1) The areas of flow instabilities in temperature contours and the regions of high value of K in contours of the value of K accord well, which reveals the physical mechanism of flow instability.

(2) The fin height and the fin space jointly dominate the flow behavior of the base flow and thus affect the heat transfer rate.

(3) For a given fin height, the change of the fin space results in the change of the accumulation and movement of the heat flux between adjacent fins, as well as the relative magnitude of heat conduction and heat convection between adjacent fins; hence the heat transfer rate changes slightly.

(4) The effect of the fin shape on heat transfer is distinct when the fin space is large.

Conflict of Interests

The authors declare that there is no conflict of interests regarding the publication of this paper.

Acknowledgments

This work is supported by the Science Foundation of Zhejiang Sci-Tech University (ZSTU) under Grant no. 11130032241201 and the special major project of science and technology of Zhejiang Province (no. 2013C01139). The authors would like to thank Associate Professor Chengwang Lei at The University of Sydney and Dr. Feng Xu in Beijing Jiaotong University for the helpful discussions. The authors also thank the support from Huadian Electric Power Research Institute.

References

[1] K. E. Starner and H. N. McManus, "An experimental investigation of free convection heat transfer from rectangular fin-arrays," *Journal of Heat Transfer*, vol. 85, no. 3, pp. 273–278, 1963.

[2] F. Harahap and H. N. McManus, "Natural convection heat transfer from horizontal rectangular fin arrays," *Journal of Heat Transfer*, vol. 89, no. 1, pp. 32–38, 1967.

[3] C. D. Jones and L. F. Smith, "Optimum arrangement of rectangular fins on horizontal surfaces for free convection heat transfer," *Journal of Heat Transfer*, vol. 92, no. 1, pp. 6–10, 1970.

[4] V. Rammohan Rao and S. P. Venkateshan, "Experimental study of freeconvection and radiation in horizontal fin arrays," *International Journal of Heat and Mass Transfer*, vol. 39, no. 4, pp. 779–789, 1996.

[5] H. Yüncü and G. Anbar, "An experimental investigation on performance of rectangular fins on a horizontal base in free convection heat transfer," *Heat and Mass Transfer*, vol. 33, no. 5-6, pp. 507–514, 1998.

[6] M. Mobedi and H. Yüncü, "A three dimensional numerical study on natural convection heat transfer from short horizontal rectangular fin array," *Heat and Mass Transfer*, vol. 39, no. 4, pp. 267–275, 2003.

[7] E. Arquis and M. Rady, "Study of natural convection heat transfer in a finned horizontal fluid layer," *International Journal of Thermal Sciences*, vol. 44, no. 1, pp. 43–52, 2005.

[8] F. Liu, "A fuzzy approach to the convective longitudinal fin array design," *International Journal of Thermal Sciences*, vol. 44, no. 3, pp. 211–217, 2005.

[9] F. Harahap, H. Lesmana, and A. S. Dirgayasa, "Measurements of heat dissipation from miniaturized vertical rectangular fin arrays under dominant natural convection conditions," *Heat and Mass Transfer*, vol. 42, no. 11, pp. 1025–1036, 2006.

[10] F. Harahap, H. Lesmana, and P. L. Sambegoro, "Concurrent calorimetric and interferometric studies of steady-state natural convection from miniaturized horizontal single plate-fin systems and plate-fin arrays," *Heat and Mass Transfer*, vol. 46, no. 8-9, pp. 929–942, 2010.

[11] M. Dogan and M. Sivrioglu, "Experimental investigation of mixed convection heat transfer from longitudinal fins in a horizontal rectangular channel," *International Journal of Heat and Mass Transfer*, vol. 53, no. 9-10, pp. 2149–2158, 2010.

[12] H. Azarkish, S. M. H. Sarvari, and A. Behzadmehr, "Optimum design of a longitudinal fin array with convection and radiation heat transfer using a genetic algorithm," *International Journal of Thermal Sciences*, vol. 49, no. 11, pp. 2222–2229, 2010.

[13] A. Giri and B. Das, "A numerical study of entry region laminar mixed convection over shrouded vertical fin arrays," *International Journal of Thermal Sciences*, vol. 60, pp. 212–224, 2012.

[14] S. Wong and G. Huang, "Parametric study on the dynamic behavior of natural convection from horizontal rectangular fin arrays," *International Journal of Heat and Mass Transfer*, vol. 60, no. 1, pp. 334–342, 2013.

[15] J. Patterson and J. Imberger, "Unsteady natural convection in a rectangular cavity," *Journal of Fluid Mechanics*, vol. 100, no. 1, pp. 65–86, 1980.

[16] H. S. Dou and N. Phan-Thien, "Instability of fluid material systems," in *Proceedings of the 15th Australasian Fluid Mechanics Conference*, The University of Sydney, Sydney, Australia, December 2004.

[17] H. S. Dou, "Viscous instability of inflectional velocity profile," in *Proceedings of the 4th International Conference on Fluid Mechanics*, Tsinghua University Press & Springer, 2004.

[18] H. Dou, "Mechanism of flow instability and transition to turbulence," *International Journal of Non-Linear Mechanics*, vol. 41, no. 4, pp. 512–517, 2006.

[19] H. S. Dou, "Three important theorems for flow stability," in *Proceedings of the 5th International Conference on Fluid Mechanics*, Tsinghua University Press & Springer, 2007.

[20] H. Dou and B. C. Khoo, "Mechanism of wall turbulence in boundary layer flow," *Modern Physics Letters B*, vol. 23, no. 3, pp. 457–460, 2009.

[21] H. Dou and B. C. Khoo, "Criteria of turbulent transition in parallel flows," *Modern Physics Letters B*, vol. 24, no. 13, pp. 1437–1440, 2010.

[22] H. Dou and B. C. Khoo, "Investigation of turbulent transition in plane couette flows using energy gradient method," *Advances in Applied Mathematics and Mechanics*, vol. 3, no. 2, pp. 165–180, 2011.

[23] H. Dou, B. C. Khoo, and K. S. Yeo, "Energy loss distribution in the plane Couette flow and the Taylor-Couette flow between concentric rotating cylinders," *International Journal of Thermal Sciences*, vol. 46, no. 3, pp. 262–275, 2007.

[24] H. Dou, B. C. Khoo, and K. S. Yeo, "Instability of Taylor-Couette flow between concentric rotating cylinders," *International Journal of Thermal Sciences*, vol. 47, no. 11, pp. 1422–1435, 2008.

[25] H. Dou, G. Jiang, and C. Lei, "Numerical simulation and stability study of natural convection in an inclined rectangular cavity," *Mathematical Problems in Engineering*, vol. 2013, Article ID 198695, 12 pages, 2013.

[26] Y. Gao, *A heat transfer study on the horizontal rectangular fin arrays for the LED street lamp GH-4 [M.S. thesis]*, Chongqing University, 2011.